Spin pumping and transport in the $Ni_{80}Fe_{20}$/Pt/Co asymmetric trilayer

Shilpa Samdani,[1] Yaqi Rong,[2] Birte Coester,[3] Amit Kumar Shukla,[1] Wen Siang Lew,[3] Yumeng Yang,[2] and Rajdeep Singh Rawat[1,*]

[1]*Natural Sciences and Science Education, National Institute of Education, Nanyang Technological University, Singapore 637616*

[2]*Shanghai Engineering Research Center of Energy Efficient and Custom AI IC, School of Information Science and Technology, ShanghaiTech University, Shanghai, 201210, China*

[3]*School of Physical and Mathematical Sciences, Nanyang Technological University, Singapore 637371*

(Received 19 April 2024; accepted 3 September 2024; published 25 October 2024)

Ferromagnet$_1$/nonmagnetic metal/ferromagnet$_2$ ($FM_1/NM/FM_2$) trilayers have garnered considerable attention because of their potential in spintronic applications. A thorough investigation of the spin transport properties of these trilayers is therefore important. Asymmetric trilayers, particularly those including platinum (Pt) as a spacer, are less explored. Pt mediates exchange coupling between the two FM layers and thus offers a unique platform to investigate the spin transport properties under indirect exchange coupling conditions through the spin-pumping mechanism. We study the static and dynamic magnetic properties of a $Ni_{80}Fe_{20}$/Pt(t)/Co trilayer system through vibrating sample magnetometry and spin pumping based on ferromagnetic resonance (FMR) spectroscopy by varying the Pt spacer thickness. Though a powerful method for characterizing the dynamic magnetic properties of FM layers, FMR is seldom the only technique used for investigating spin transport characteristics of asymmetric trilayers. Our analytical focus on the acoustic mode, facilitated by the distinct magnetizations of the $Ni_{80}Fe_{20}$ and Co layers, allows for the isolation of individual layer resonances. The derived spin pumping induced damping (α_{sp}) of the $Ni_{80}Fe_{20}$ and Co layers reveals a direct dependence on the Pt spacer thickness. Furthermore, fitting of the weighted average of the damping parameters to the α_{sp} of the acoustic mode reveals that the observed FMR spectra are indeed a result of the in-phase precession of the magnetizations in two FM layers. The extracted effective spin-mixing conductance ($g_{eff}^{\uparrow\downarrow}$) varies with the FM/NM interface, specifically 1.72×10^{19} m^{-2} at the $Ni_{80}Fe_{20}$/Pt interface and 4.07×10^{19} m^{-2} at the Co/Pt interface, indicating a strong correlation with interfacial characteristics. Additionally, we deduce the spin diffusion length in Pt to be between 1.02 and 1.55 nm and calculate the interfacial spin transparency (T_{in}) and spin current densities, highlighting significant disparities between the $Ni_{80}Fe_{20}$/Pt and Co/Pt interfaces. This detailed analysis enhances our understanding of the spin transport in $Ni_{80}Fe_{20}$/Pt/Co trilayers. It offers insights important for advancing spintronic device design and lays the groundwork for future theoretical investigations of asymmetric trilayer systems.

DOI: 10.1103/PhysRevB.110.134440

I. INTRODUCTION

Trilayer systems consisting of two ferromagnetic (FM) layers separated by a nonmagnetic (NM) layer have attracted the interest of the magnetism and spintronics research community since the discovery of the giant magnetoresistance (GMR) effect in the 1990s. Traditionally, trilayers have been studied for applications in magnetic recording and random memories. In recent years, a renewed interest in these trilayers has been seen in emerging areas of spintronics studies such as field-free spin-orbit torque switching [1], spin-torque microwave nanodevices [2–4], and synthetic antiferromagnetic devices [5,6]. Understanding the transfer of pure spin current [7,8] in the trilayers, in other words the "spin transport," is important for the development of low-power and high-speed spintronic devices. Investigating the magnetization dynamics of the FM layer makes it possible to gain direct insight into important spin transport properties such as the spin-diffusion length (λ_{sd}) and the spin-mixing conductance ($g_{\uparrow\downarrow}$). λ_{sd} is the characteristic length which the pure spin current traverses in the NM layer before dissipating via spin-flip processes while $g_{\uparrow\downarrow}$ parametrizes the efficiency of spin transport across the FM/NM interface [9].

In the case of a symmetric coupled trilayer, i.e., when both the FM layers are of the same material (FM/NM/FM), it is straightforward to obtain the value of spin-mixing conductance ($g_{\uparrow\downarrow}$) at the FM/NM interface by studying the collective magnetization dynamics of the coupled FMs, such as Fe/Ag/Fe [10], NiFe/Pt/NiFe [11], etc. However, complexity arises when the trilayer system is asymmetric, i.e., when the two FM layers are different ($FM_1/NM/FM_2$), because the two different FM/NM interfaces result in two different values of $g_{\uparrow\downarrow}$. The differing values of $g_{\uparrow\downarrow}$ in turn result in directional asymmetry in the spin current pumped from FM_1 and FM_2 and transported into the NM spacer layer. Therefore, to correctly describe the spin transport in asymmetric trilayers it is important to quantify the $g_{\uparrow\downarrow}$ at each FM/NM interface.

To date, various approaches including nonlocal magnetotransport [12], inverse spin Hall effect (ISHE)

*Contact author: rajdeep.rawat@nie.edu.sg

[13], and spin-torque ferromagnetic resonance (STFMR) [14] have been used to investigate spin transport properties. Lithography-free approaches such as broadband ferromagnetic resonance (FMR) and x-ray detected FMR (XFMR) based spin pumping and time resolved magneto-optical Kerr effect (TRMOKE) offer an easier route to investigate the pure spin current transport. Hitherto, reports on the investigation of spin transport in asymmetric trilayers by such approaches are rather scarce; they include systems such as synthetic antiferromagnetic (SAF) heterostructures, for example, FeCoV/Ru/NiFe [15] and $[Co/Pd/Co]_{FM_1}/[Ru/Ta]_{NM}/CoFeB_{FM_2}$ [16], spin transfer torque–magnetic tunnel junctions (STTMTJs) CoFeB/Ta/NiFe [17], spin-valve Co/Cu/CoFeB [18], CoFe/Cr/NiFe [19], and novel heterostructures $CoFe/Bi_2Se_3/NiFe$ [20]. We note that, though FMR is a powerful technique that allows extraction of dynamic magnetic properties such as the effective demagnetizing field, interfacial magnetic anisotropy, and the damping parameter, it is rare to find studies where broadband FMR is exclusively utilized to probe spin transport in trilayer configurations. Typically, it is combined with XFMR for a detailed examination of each FM layer's resonant properties independently. However, the distinct bulk magnetizations of the two different FM layers in an asymmetrical trilayer system provide an opportunity for resonance deconvolution through line shape analysis. Furthermore, there are very few reports on the spin pumping in platinum (Pt) in asymmetric trilayer systems, making the $FM_1/Pt/FM_2$ heterostructure a novel and compelling system for investigation.

At the FM/Pt interface a finite magnetic moment emerges due to direct exchange coupling, affecting up to few atomic layers of Pt [21]. Additionally, in FM/Pt/FM trilayers there exists a static indirect exchange coupling (IEC) between the FMs. The strength of this coupling diminishes exponentially with the increase in the thickness of the Pt layer [22–25]. The presence of IEC fosters the hybridization of the magnetization precession in the two FM layers resulting in two distinct modes: an in-phase (or acoustic) mode and an out of phase (or optical) mode. It is observed that damping of the optical mode is higher than the acoustic mode [11,26–28] rendering it challenging to observe the optical mode in experiments [29,30]. In coupled $FM_1/NM/FM_2$ systems, spin pumping induces dynamic coupling between the FM layers. This happens as a result of the spin currents being simultaneously ejected from both the FMs and being nonlocally dampened [31]. The absorption of the incoming spin current balances the loss of angular momentum when the magnetizations precess in phase, but this loss is amplified when the precession is out of phase. Consequently, the spin pumping induced damping is dependent on the precessing magnetizations' phase and amplitude [32].

We present a comprehensive study of the static and dynamic magnetic properties alongside the spin transport characteristics within an asymmetric trilayer $Ni_{80}Fe_{20}/Pt(t)/Co$ system employing broadband FMR spectroscopy and vibrating sample magnetometry (VSM). By varying the thickness of the Pt spacer layer, we aim to modulate and examine the IEC between the FM layers and its subsequent effect on the magnetization dynamics of the two FM layers. The focal point of our investigation is the acoustic mode of the trilayer system, which, due to the differing bulk magnetizations of the two FM layers, enables the deconvolution and individual resonance analysis of each FM layer through line-shape analysis. Our methodological approach is similar to that of Omelchenko *et al.* [11], the distinguishing factor being that we study an asymmetric trilayer system and subsequently extend the analysis to isolate the separate spin-mixing conductances of the two interfaces. Through FMR and VSM, we extracted key parameters such as the damping coefficient and coupling strength, respectively. Our analysis reveals the dependency of spin pumping induced damping of the specific FM layers and $g_{\uparrow\downarrow}$ on the respective FM/Pt interface. Additionally, we quantified the interfacial spin transparency and spin current density at each FM/Pt interface. The interfacial spin transparency of the trilayer is found to match the FM/Pt bilayer and the spin current density is observed to be dependent on the Pt spacer thickness.

II. EXPERIMENTAL DETAILS

Thin films were deposited at ambient temperature on thermally oxidized single-crystalline Si substrates utilizing magnetron sputtering. The deposition was carried out in Ar atmosphere at a chamber base pressure greater than 4×10^{-7} Torr. The deposited multilayer sequence was as follows: Si substrate//Ta(2)/$Ni_{80}Fe_{20}$(6 nm)/Pt(t_{NM})/Co(6 nm)/Ta (2 nm), where the thickness of the Pt layer (t_{NM}) was varied across samples—specifically, 0, 0.5, 1.5, 3.5, and 7 nm. To simplify discussions, samples are henceforth designated based on their Pt layer thickness as Pt(0), Pt(1.5), Pt(3.5), and Pt(7), respectively. An underlayer and capping layer of Ta were deposited to promote uniform film growth of $Ni_{80}Fe_{20}$ and prevent the oxidation of the Co layer, respectively. Additionally, a control sample using a spacer layer of Cu(7) was fabricated and analyzed to underscore the distinctive effects attributable to Pt. The samples are polycrystalline; x-ray characterization of Pt(0.5) and Pt(1.5) is shown in the Supplemental Material, Sec. S-I [33].

Broadband, field-swept, in-plane magnetic field, ferromagnetic resonance (FMR) measurements were conducted using a Quantum Design VersaLab system with a coplanar waveguide and NanoOsc Phase FMR lock-in detection. Experiments spanned a frequency range of 5–20 GHz, with an external dc magnetic field oriented parallel to the sample plane. Samples were saturated at 15 kOe, well above the magnetic field sweep used, to ensure full saturation during measurements. Static magnetic properties were characterized using vibrating sample magnetometry (VSM) on the Quantum Design VersaLab system. These measurements were performed at room temperature, applying fields up to 6 kOe in an in-plane configuration. For samples comprising multiple ferromagnetic (FM) layers, such as the $FM_1/NM/FM_2$ structures discussed in this study, the observed hysteresis loops are derived from the collective magnetic responses of both the involved FM layers.

III. STATIC MAGNETIC PROPERTIES

Figure 1(a) displays the in-plane hysteresis loops that demonstrate the magnetization reorientation transition for

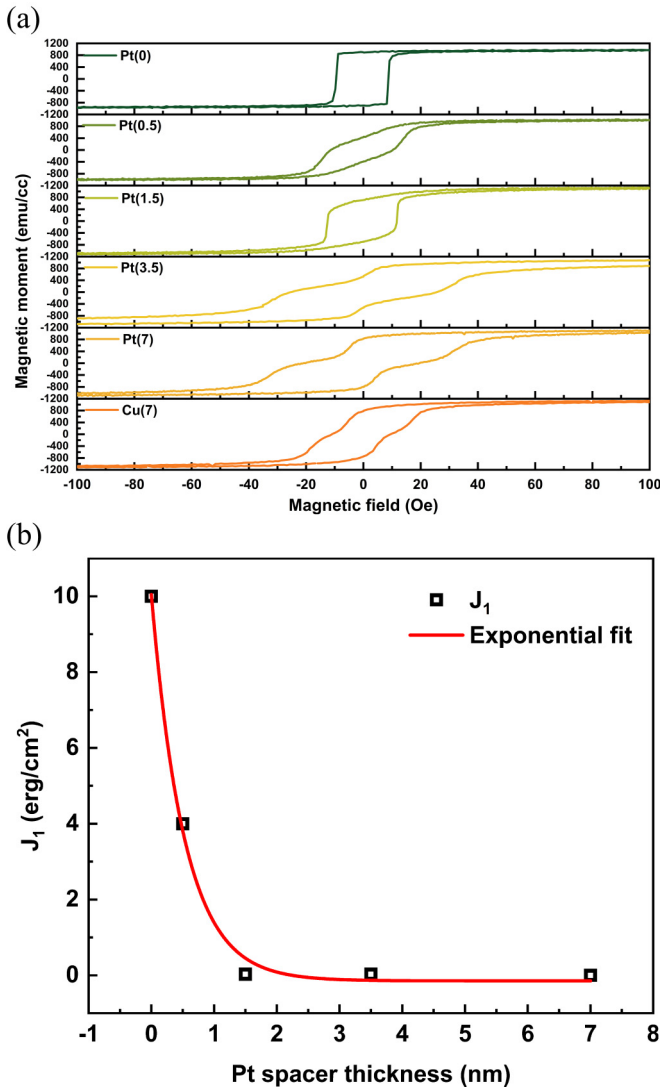

FIG. 1. (a) In-plane hysteresis loops of $Ni_{80}Fe_{20}$(6 nm)/NM (t nm)/Co(6 nm) trilayers with NM spacers—Pt(0, 0.5, 1.5, 3.5, and 7 nm) and Cu(7 nm), and (b) the variation in coupling strength, J_1, as a function of the Pt spacer thickness.

a series of $Ni_{80}Fe_{20}(6)/Pt(t)/Co(6)$ trilayer samples. The thickness, t_{NM}, of the Pt spacer varies from 0 to 7 nm. The Pt(0) sample exhibits a square loop with a unique switching field, suggesting that the two ferromagnetic layers are acting synergistically as a single composite entity. This observation is indicative of strong coupling between the FM layers, primarily through direct exchange interactions. The phenomena of IEC in samples with ultrathin NM spacers, such as for Pt(0.5) and Pt(1.5) samples, can be attributed to one or a combination of phenomena, including the Ruderman-Kittel-Kasuya-Yosida (RKKY) interaction [34], direct exchange coupling via pinholes in the spacer layer [35] and the magnetic proximity effect in Pt [36]. An early magnetization reversal in Pt(3.5), Pt(7), and Cu(7) samples also hints at the presence of magnetostatic (dipole-dipole) coupling [37], prompting a premature reorientation of magnetic moments in the softer FM layer in response to the external magnetic field's directional shifts. The Supplemental Material, Sec. S-I [33], provides a detailed analysis of how the thickness of the Pt spacer layer affects the intrinsic coercive field (H_{ic}) and the saturation magnetization (M_s).

The coupling strength (J_1) obtained from the macrospin simulations—refer to the Supplemental Material, Sec. S-II [33]—is shown in Fig. 1(b). It can be modeled as exponentially changing with Pt thickness, with J_1 diminishing to nearly zero for $t_{Pt} \geqslant 1.5$ nm. This relationship between coupling strength and spacer thickness is consistent with findings in other coupled trilayer systems such as Co/Pt/Co [24], FeNi/Cu/FeCo [38], and Fe/Pd/Fe [39], suggesting a universal trend across various material compositions. Specifics regarding the energy equation and simulated M-H loops values are provided in the Supplemental Material, Sec. S-II [33].

IV. DYNAMIC MAGNETIC PROPERTIES

Broadband FMR spectroscopy is a widely used technique for investigating spin current, enabling the indirect quantification of spin current by analyzing the enhancement in the Gilbert damping parameter [40,41]. This technique reveals how the IEC influences the effective magnetic field of the coupled FM layers in a trilayer system, manifesting as a shift in the resonance peak position as seen later in Fig. 3(a).

To elucidate the effect of interlayer coupling on the spin pumping in our trilayer system, we investigated the dynamic properties of the magnetization by measuring the derivative (dI/dH) of the FMR spectra. Figure 2(a) shows a schematic of flip-chip FMR measurement configuration. The in-phase precession of the magnetizations of Co and $Ni_{80}Fe_{20}$ when FMs are coupled, and the independent precession in the case of decoupled FMs, alongside the simultaneous spin pumping into Pt, are represented schematically in Figs. 2(b)–2(d). The acquired signal is fitted to the derivative of the Lorentzian function.

The fitting equation applied in our study is structured as follows.

$$\frac{dI}{dH} = S_1\left[\frac{\frac{\Delta H_1}{2}(H-H_{res,1})}{\left[(H-H_{res1})^2+\left(\frac{\Delta H_1}{2}\right)^2\right]^2}\right] + A_1\left[\frac{\left(\frac{\Delta H_1}{2}\right)^2-(H-H_{res,1})}{\left[(H-H_{res1})^2+\left(\frac{\Delta H_1}{2}\right)^2\right]^2}\right] + \text{offset} + S_2\left[\frac{\frac{\Delta H_2}{2}(H-H_{res,2})}{\left[(H-H_{res,2})^2+\left(\frac{\Delta H_2}{2}\right)^2\right]^2}\right] + A_2\left[\frac{\left(\frac{\Delta H_2}{2}\right)^2-(H-H_{res,2})}{\left[(H-H_{res,2})^2+\left(\frac{\Delta H_2}{2}\right)^2\right]^2}\right] + Hm, \quad (1)$$

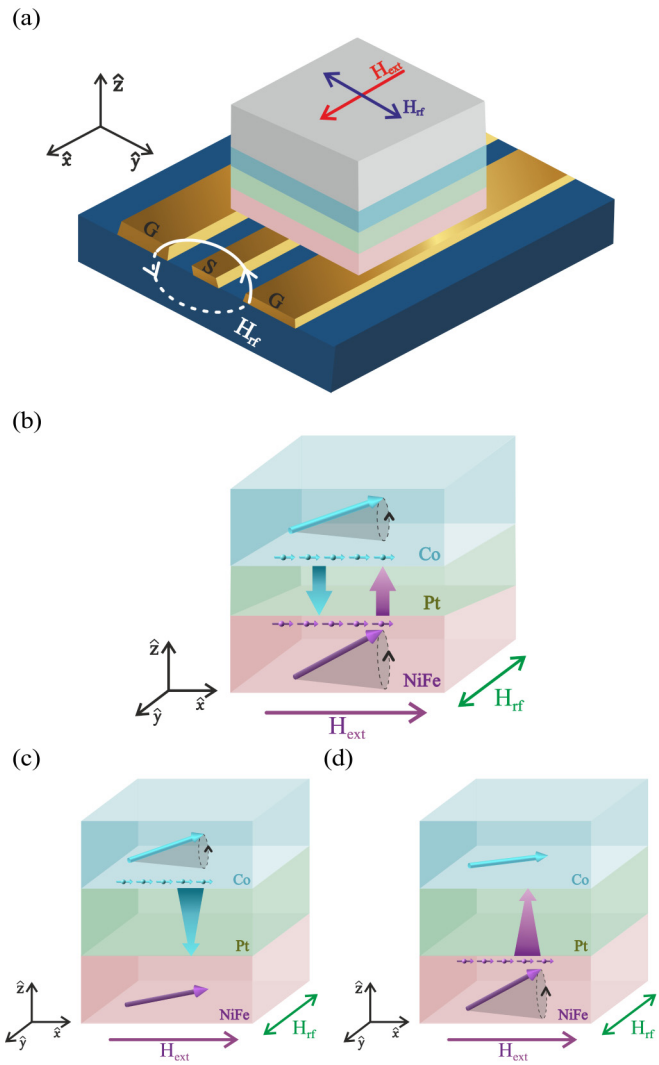

FIG. 2. Schematic of (a) configuration of flip-chip coplanar waveguide ferromagnetic resonance spectroscopy with an in-plane magnetic field (red arrow), (b) $FM_1/NM/FM_2$ trilayer of $Ni_{80}Fe_{20}$/Pt/Co showing the in-phase precession of magnetizations of Co and $Ni_{80}Fe_{20}$ layers accompanied by spin pumping in Pt spacer layer; $t_{Pt} = 0.5$ and 1.5 nm. When $t_{Pt} = 3.5$ and 7 nm (c) represents spin pumping of Co and (d) represents spin pumping of $Ni_{80}Fe_{20}$. Cyan and purple arrows in Co and $Ni_{80}Fe_{20}$ layers represent the precessing bulk magnetization. The electron spins in Co (cyan) and $Ni_{80}Fe_{20}$ (purple) represent the ejected spin current. Arrows in the Pt spacer represent the spin current transport in the Pt spacer. The spin current pumped by Co and $Ni_{80}Fe_{20}$ is represented by the cyan and purple arrows, respectively. Depending on Pt layer thickness the spin current undergoes either ballistic ($t_{Pt} < \lambda_{sd}$) or diffusive ($t_{Pt} > \lambda_{sd}$) transport.

where ΔH_1 and ΔH_2 represent the resonance linewidths and H_{res1} and H_{res2} represent the resonance magnetic fields of the FM_1 and FM_2 layers, respectively; m is the slope; and S and A are amplitudes of the Lorentzian fitting function. Figure 3(a) shows the typical field-swept FMR spectra for the various samples, $Ni_{80}Fe_20(6)/Pt(t)/Co(6)$ and $Ni_{80}Fe_{20}(6)/Cu(7)/Co(6)$, all measured at 20 GHz. The experimental data are well fitted to Eq. (1) facilitating the precise determination of the resonance

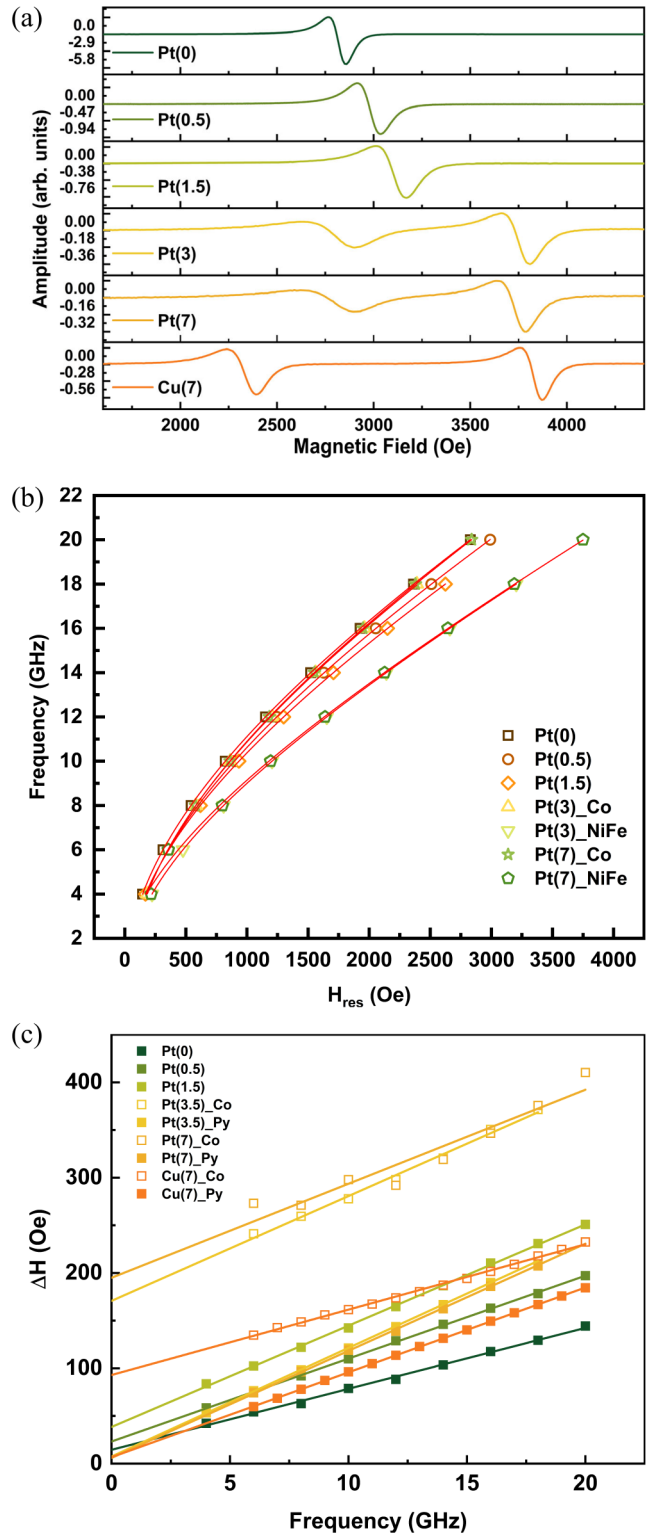

FIG. 3. (a) FMR spectra measured at 20 GHz for all the samples, (b) rf excitation frequency vs resonance field (H_{res}); solid lines are fits using the Kittel equation using Eq. (2). For decoupled trilayers, data for both NiFe and Co layers are shown, and (c) ferromagnetic resonance linewidth, ΔH, as a function of frequency for varying thickness of Pt spacer; hollow and solid squares represent the linewidth of Co and $Ni_{80}Fe_{20}$ layers, respectively. Solid lines represent fit using Eq. (3) to extract the effective Gilbert damping parameter.

field (H_{res}) and linewidth (ΔH). When the FM layers are strongly coupled ($t_{Pt} = 0,\ 0.5,\ 1.5$ nm) a single FMR peak is observed. This peak exhibits a decrease in intensity and an increase in linewidth, alongside a shift to higher magnetic fields as the spacer layer thickness increases. Conversely, for weakly coupled or decoupled FMs, exemplified by $t_{Pt} = 3.5$ nm, 7 nm and $t_{Cu} = 7$ nm, two distinct resonance peaks emerge, each representing the independent precession of magnetization within the two FM layers. These findings corroborate the insights related to coupling of the two FM layers, gained from examining the static magnetization characteristic in the preceding analysis.

The effective magnetization ($4\pi M_{eff}$) was calculated by fitting the frequency vs H_{res} data, shown in Fig. 3(b), to the Kittel's equation for in-plane configuration of FMR as described by Eq. (2). This equation is obtained by solving the Landau-Lifshitz-Gilbert (LLG) equation in the small-angle precession limit of magnetization.

$$f = \frac{\gamma}{2\pi}[(H_{res} + H_k)(H_{res} + H_k + 4\pi M_{eff})]^{1/2}, \qquad (2)$$

where f represents the resonance frequency, γ the gyromagnetic ratio with $\gamma = g\mu_B/\hbar = g \times 87.94$ Hz/T, H_{res} the resonance field, and H_k is the in-plane anisotropy field. Given typical values for Co and NiFe g factors as 2.18 and 2.1, respectively, we observed that in weakly coupled or decoupled samples ($t_{Pt} = 3$ and 7 nm and $t_{Cu} = 7$ nm) the effective magnetization ($4\pi M_{eff}$) for the initial peak at lower magnetic field and the subsequent peak at higher magnetic field measure approximately 12–13.5 kOe and 8.1 kOe, respectively. These findings distinctly attribute the initial and subsequent peaks to the ferromagnetic resonances of Co and NiFe, respectively.

Figure 3(c) shows the dependence of the linewidths (ΔH) of the Co and $Ni_{80}Fe_{20}$ resonance peaks on the FMR excitation frequency across different Pt spacer thicknesses; hollow and solid squares represent the linewidth of Co and $Ni_{80}Fe_{20}$ layers, respectively. The linear variation in linewidth as a function of frequency for all the samples indicates the intrinsic origin of damping. From the linear correlation between the ΔH and frequency, we deduce the effective damping parameter (α_{eff}) and the linewidth broadening due to inhomogeneities in the film (ΔH_0) [42,43]:

$$\Delta H = \frac{4\pi\alpha_{eff}}{\gamma} f + \Delta H_0. \qquad (3)$$

ΔH_0 is also referred to as the zero-frequency broadening is the lowest for $Ni_{80}Fe_{20}$ in Pt(7) sample at ~6 Oe. It increases with t_{Pt} while the reverse trend is seen in the ΔH_0 Co peak as in the trilayer with Pt(7) ~194 Oe, and 30 Oe for the Pt(0) sample. These values are on the higher side as compared to other reports of a $Ni_{80}Fe_{20}$ symmetric trilayer system with a Pt spacer [11]. The solid lines in Fig. 3(b) represent linear fits to the data. From the slope of Eq. (3) we determine the effective Gilbert damping parameter, which subsequently allows us to extract the spin pumping induced damping as shown later in Fig. 4.

Further analysis of the FMR spectra concerning the effective magnetization and interfacial anisotropy is discussed in the Supplemental Material, Sec. S-III [33]. We have thus investigated the features and origin of the obtained FMR spectra. We now discuss the main results related to the dynamic magnetic properties of each FM layer and spin transport across each FM/NM interface, starting with the relaxation dynamics at each FM/Pt interface.

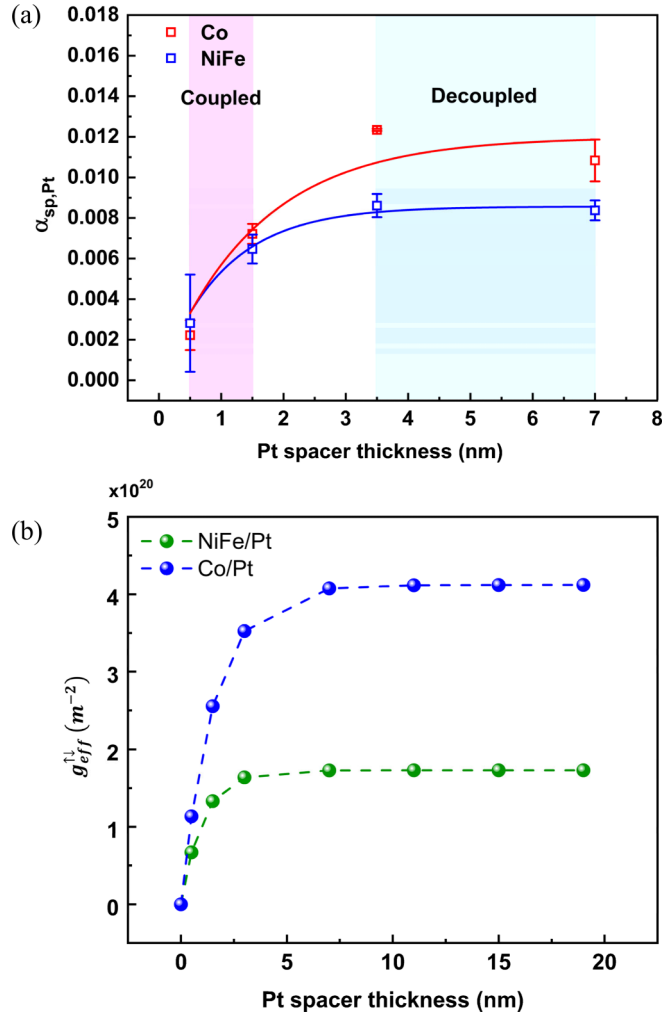

FIG. 4. (a) Spin pumping induced damping at $Ni_{80}Fe_{20}$/Pt and Co/Pt interfaces as a function of spacer thickness; solid line represents the fit by spin-pumping model using Eq. (4) to extract the spin-diffusion length (λ_{sd}) and intrinsic spin-mixing conductance ($g_{int}^{\uparrow\downarrow}$), (b) Effective spin-mixing conductance as a function of Pt spacer thickness calculated using Eq. (5). Dashed line is a guide to the eye.

V. SPIN PUMPING AND SPIN TRANSPORT

Spin pumping refers to the phenomenon of the transfer of spin current by a precessing magnetization to the neighboring NM layer because of the nonequilibrium spin accumulation in the FM layer. This process is an outcome of the dynamic and coherent precession of the magnetization around the effective magnetic field (H_{eff}) in a FM layer. H_{eff} includes the external magnetic field, crystal anisotropy, and demagnetizing fields. The enhancement in the damping of the amplitude of precession of magnetization in the FM layer is understood to be a

direct consequence of this spin-pumping phenomenon [40]. The damping of the precessing magnetization is enhanced when the spin current that leaks out of the FM layer dissipates via spin-flip processes in the NM layer after traveling a distance greater than the spin-diffusion length (λ_{sd}) of the NM layer. However, when $t_{NM} < \lambda_{sd}$, spin accumulation at the FM/NM interface leads to a backflow of the spin current in the FM. Thus the total spin current at the FM/NM interface can be described as a sum of spin current due to spin pumping from FM (I_s^{pump}) into the NM and backflow spin current from NM into the FM (I_s^{back}). In coupled trilayer systems, $FM_1/NM/FM_2$, the backflow spin current at the FM_1/NM interface also includes spin currents pumped out of FM_2 and vice versa. Furthermore, the damping of the precessing magnetization in FM_1 (FM_2) also depends on the phase of the spin current pumped out of FM_2 (FM_1). We reserve further discussion on the phase difference of precessing magnetization and its effect on damping until Sec. VI.

The intrinsic spin-mixing conductance ($g_{int}^{\uparrow\downarrow}$) of a FM/NM interface is a measure of the inherent efficiency of the FM/NM interface in facilitating the transfer of spin angular momentum from the FM to the NM layer, independent of the spin backflow. $g_{int}^{\uparrow\downarrow}$ is determined from the variation of spin pumping induced damping (α_{sp}) as a function of NM thickness (t_{NM}). Spin-mixing conductance correlates spin pumping to the intrinsic properties of the FM and the experimentally measurable effective Gilbert damping parameter, which as outlined earlier, is directly affected by the phenomenon of spin pumping. It is given as follows [44]:

$$\alpha_{sp} = g_{int}^{\uparrow\downarrow} \frac{g\mu_B(1 - e^{(-t_{NM})/\lambda_{sd}})}{4\pi M_s t_{FM}}, \tag{4}$$

where all symbols hold their usual meaning. In FM/NM systems the exponential term in the above equation describes the spin diffusion in NM and accounts for the attenuation of spin current as it diffuses through the NM material. To realistically model the spin transport phenomena, the exponential decay term for $t_{NM} < \lambda_{sd}$ is typically multiplied by a factor of 2 that signifies the distance traversed by the spins after reflection from the NM/air interface, which is assumed to be a perfect spin reflector [45]. However, considering the earlier provided physical explanation of the spin dynamics at the interface in a trilayer, we exclude the factor of 2 from our analysis of the $FM_1/NM/FM_2$ system, operating under the assumption that the FM layers act as a perfect spin sink. This assumption has certain limitations. Firstly it is important to note that when the thickness of the NM spacer is comparable to or less than the λ_{sd}, though spins can transit through the interlayer, the transport is only partly ballistic as diffused scattering and backflow occurs at the NM/FM interfaces [10]. Additionally, the uniform spin diffusion does not account for the microstructural inhomogeneities in the NM layer, spin lifetime, and mean free path which may also lead to nonuniform spin diffusion across its thickness. Ignoring these factors may lead to overestimation of the spin current reaching the NM/FM_2 interface and λ_{sd}.

Furthermore, the perfect spin sink behavior attributed to FM_2, does not consider factors such as magnetic alignment, interface quality, and FM layer thickness which may cause deviations in the ideal spin sink behavior when the FM layers are decoupled and contribute to backflow of spins in FM_1 or scattering in the spacer layer.

On the other hand, when accounting for the spin backflow, the efficiency of spin pumping across the FM/NM interface is given by the effective complex spin-mixing conductance ($g_{eff}^{\uparrow\downarrow}$) per unit area of the interface. It is expressed as $g_{eff}^{\uparrow\downarrow} = \mathrm{Re}(g_{eff}^{\uparrow\downarrow}) + \mathrm{Im}(g_{eff}^{\uparrow\downarrow})$. In the nonmagnetic metal layer, the imaginary component of the complex effective spin-mixing conductance is significantly smaller than the real part [40,46]. The real part, which primarily influences the efficiency of spin transfer across the FM/NM interfaces, is closely associated with the intrinsic spin-mixing conductance in the following manner [44,45]:

$$g_{eff}^{\uparrow\downarrow} = g_{int}^{\uparrow\downarrow}(1 - e^{\frac{-t}{\lambda_{sd}}}). \tag{5}$$

As the effective spin-mixing conductance offers valuable insights into the interfacial spin transfer characteristics it is an important parameter to consider when developing spintronic devices with one or more FM/NM layers.

In Eq. (4), the term α_{sp} is derived from α_{eff} which encapsulates all the contributions to the experimentally measured damping such as the intrinsic damping (α_{int}) of the FM layer and the additional damping resulting from spin pumping. α_{eff} can be given as follows [47]:

$$\alpha_{eff} = \alpha_{int} + \alpha_{sp}. \tag{6}$$

We note that in addition to the spin pumping in Pt the seed and capping NM layers also contribute to the spin pumping. Therefore, to extract the spin-pumping damping in Pt we must separate these additional contributions. Accordingly, Eq. (6) can be rewritten for the $Ni_{80}Fe_{20}$ and Co layers as the following Eqs. (7) and (8), respectively.

$$\alpha_{eff,\ NiFe} = \alpha_{NiFe} + \alpha_{sp,seed} + \alpha_{sp,Pt}, \tag{7}$$

$$\alpha_{eff,\ Co} = \alpha_{Co} + \alpha_{sp,cap} + \alpha_{sp,Pt}, \tag{8}$$

where α_{NiFe} and α_{Co} represent the intrinsic damping of $Ni_{80}Fe_{20}$ and Co layers, respectively; $\alpha_{sp,seed}$ and $\alpha_{sp,cap}$ represent the damping in seed and capping layers, respectively; and $\alpha_{sp,Pt}$ is the damping due to spin pumping in Pt.

The general form can be written as follows:

$$\alpha_{eff} = \alpha_{ref} + \alpha_{sp,Pt}. \tag{9}$$

α_{ref} is the reference damping due to both the intrinsic and extrinsic sources. This equation thus accounts for the diverse sources of damping. We separately found α_{ref} for the $Ta(2)/Ni_{80}Fe_{20}(6)/Cu(3)$ and $Co(6)/Ta(2)$ layers to be 8.21×10^{-3} and 5.7×10^{-3}, respectively. The linewidth as a function of frequency for the isolated layers of the Co and NiFe reference layers is shown in the Supplemental Material, Sec. S-IV [33].

The variation of $\alpha_{sp,Pt}$ as a function of Pt spacer thickness for $Ni_{80}Fe_{20}$ and Co is shown in Fig. 4(a). The value of $\alpha_{sp,Pt}$ increases with t_{Pt} and reaches different values of saturation for the two FM layers; 7.8×10^{-3} for $Ni_{80}Fe_{20}$ and up to 12×10^{-3} for Co. A higher value of damping for Co indicates a larger transfer of spin angular momentum out of the precessing FM through its interface with the adjacent NM

TABLE I. Estimated effective spin-mixing conductance and spin diffusion length at $Ni_{80}Fe_{20}$/Pt and Co/Pt, in the context of the literature.

$g_{\text{eff}}^{\uparrow\downarrow}(\text{m}^{-2})$ ($Ni_{80}Fe_{20}$/Pt interface)	$g_{\text{eff}}^{\uparrow\downarrow}(\text{m}^{-2})$ (Co/Pt interface)	λ_{sd}(m)
1.72×10^{19}	4.07×10^{19}	$1.02 \times 10^{-9} \pm 1.4 \times 10^{-10}$ ($Ni_{80}Fe_{20}$/Pt) 1.55×10^{-9} (Co/Pt)
This work	This work	This work
1.08×10^{20} [49]	$3.96 \times 10^{19} \pm 3.9 \times 10^{18}$ [50]	$1.1 \times 10^{-9} \pm 6.0 \times 10^{-10}$ [11]
$1.52 \times 10^{19} \pm 3.4 \times 10^{18}$ [50]	4.5×10^{19} [51]	1.4×10^{-9} [14,52]
2.1×10^{19} [53]		1.5×10^{-9} [54]
2.4×10^{19} [55]		2.4×10^{-9} [56]
4.0×10^{19} [51]		
$4.3 \times 10^{19} \pm 4 \times 10^{18}$ [11]		

[40] and a faster relaxation of precession in Co as compared to $Ni_{80}Fe_{20}$ in the decoupled regime. A mutual transfer of spin angular momentum between the two FM layers results in nearly equal relaxation rates in the coupled regime [17]. With a Cu(7) spacer, $\alpha_{sp,Pt}$, measured 4.3×10^{-3} and 4.7×10^{-3} for Co and $Ni_{80}Fe_{20}$, respectively, are lower than the values obtained for Pt. This difference can be attributed to the magnetic proximity effect at the FM/Pt interface [48]. The magnetic proximity effect refers to the induction of magnetic order by the FM layer in the neighboring NM layer at their interface. Its effect at the FM/Pt interface is significantly higher than that at the FM/Cu interface because firstly Pt has stronger SOC than Cu and secondly the Pt has partially filled d orbitals, compared to a fully filled d orbital for Cu, which allows greater interaction with d-orbital electrons of the FM layer. This result suggests that by considering the magnetic proximity effects at the FM/NM interface we can design spacer layers to tune the transfer of spin current in devices.

The solid lines in Fig. 4 show the curve fitting of $\alpha_{sp,Pt}$ using Eq. (4) for $Ni_{80}Fe_{20}$ and Co. The derived values of $g_{\text{int}}^{\uparrow\downarrow}$ at the $Ni_{80}Fe_{20}$/Pt and Co/Pt interfaces are $1.73 \times 10^{19}(\pm 4.5 \times 10^{17})$ and $4.12 \times 10^{19}(\pm 5.3 \times 10^{18})$, respectively, while the λ_{sd} values of Pt are found to be $1.02 \times 10^{-9}(\pm 1.4 \times 10^{-10})$ and $1.55 \times 10^{-9}(\pm 6.0 \times 10^{-10})$ from the fitting of the $Ni_{80}Fe_{20}$ and Co data, respectively. These values lie in the range reported for bilayer and trilayer heterostructures of Pt as seen in Table I.

Figure 4(b) shows the variation in the effective spin-mixing conductance ($g_{\text{eff}}^{\uparrow\downarrow}$) of the trilayers, calculated using Eq. (5), as a function of Pt spacer thickness for $Ni_{80}Fe_{20}$/Pt and Co/Pt interfaces. It indicates change in the efficiency of spin current transfer with respect to the spacer thickness. As expected from Eq. (5), $g_{\text{eff}}^{\uparrow\downarrow}$ increases with Pt thickness and for $t_{\text{NM}} \gg \lambda_{sd}$, its value saturates at $g_{\text{int}}^{\uparrow\downarrow}$. This result shows how the spacer material approaches ideal interface characteristics as the spin backflow is compensated by the spin scattering in Pt.

Using Eq. (5), we determined $g_{\text{eff}}^{\uparrow\downarrow}$; the values that we obtain are tabulated in Table I and are found to be consistent with those reported in the literature. The slight variation in the values of the spin-mixing conductance and spin-diffusion length, in comparison with cited references, can stem from several sources such as the interface quality, due to the difference in the deposition conditions, that may affect the interfacial spin scattering and transmission efficiency and even the measurement technique employed, such as FMR, ISHE, and STFMR which on account of the different sources of errors and experimental sensitivity can affect the estimated values.

Consistent with our findings, the phenomenon of nonreciprocal spin-pumping damping characterized by varying spin-mixing conductance values and their dependency on spacer thickness has been identified in FeCoV/Ru/NiFe asymmetric trilayers as well, with higher spin-mixing conductance values reported for NiFe/Ru interface in trilayers ranging from $(11.7-7.7) \times 10^{19}\text{m}^{-2}$ compared to the NiFe/Ru bilayer $\sim (3.9 \pm 0.3) \times 10^{19}$ m^{-2} [15]. This variation indicates the significant role of trilayer configurations in modulating the spin-mixing conductance. While a recent work in the literature has touched upon reciprocal spin pumping induced damping in asymmetric trilayers [16], however, our observations distinctly demonstrate the nonreciprocal nature of α_{sp} across different FM layers, further emphasizing the complexity of spin interactions in such engineered heterostructures.

From the point of view of generation, manipulation, and detection of spin currents for different spintronic applications, it is important to quantify the interfacial spin transparency ($T_{\text{FM/Pt}}$) for the FM/Pt interface. For example, in magnetic memories, spin filter, and spin valves understanding $T_{\text{FM/Pt}}$ can significantly enhance the efficiency, maximize the spin polarized current, etc. $T_{\text{FM/Pt}}$ essentially measures the impedance to spin current flow at the interface, influenced by electronic state mismatch and lattice imperfections. It is directly related to the effective spin-mixing conductance ($g_{\text{eff}}^{\uparrow\downarrow}$) as follows [45,50]:

$$T_{\text{FM/Pt}} = \frac{g_{\text{eff}}^{\uparrow\downarrow}\tanh\left(\frac{t}{2\lambda}\right)}{g_{\text{eff}}^{\uparrow\downarrow}\coth\left(\frac{t}{\lambda_{sd}}\right) + \frac{h}{2\lambda e^2 \rho}}, \tag{10}$$

where ρ (= 20 μΩ cm) [50]; t and λ are the resistivity, thickness, and spin-diffusion length of Pt. $T_{\text{Co/Pt}}$ is found to be ~62% and $T_{\text{NiFe/Pt}} \sim 25\%$. Both values are in agreement with the reported values for Co/Pt and $Ni_{80}Fe_{20}$/Pt interfaces [50]. The higher $T_{\text{FM/Pt}}$ observed at the Co/Pt interface suggests a more conducive pathway for spin current flow in comparison to the $Ni_{80}Fe_{20}$/Pt interface.

Based on phenomenological model of spin pumping, the interfacial spin current density ($j_s^{\text{FM/Pt}}$) has been related to the effective Gilbert damping parameter, α_{eff}, and NM material dependent spin-mixing conductance $g_{\text{eff}}^{\uparrow\downarrow}$(Pt) [44,57]:

$$j_s^{\text{FM/Pt}} = \frac{g_{\text{eff}}^{\uparrow\downarrow}(Pt)\gamma^2 h_{rf}^2 \hbar[4\pi M_s\gamma + \sqrt{(4\pi M_s)^2\gamma^2 + 4\omega^2}]}{8\pi\alpha_{\text{eff}}^2[(4\pi M_s)^2\gamma^2 + 4\omega^2]}. \tag{11}$$

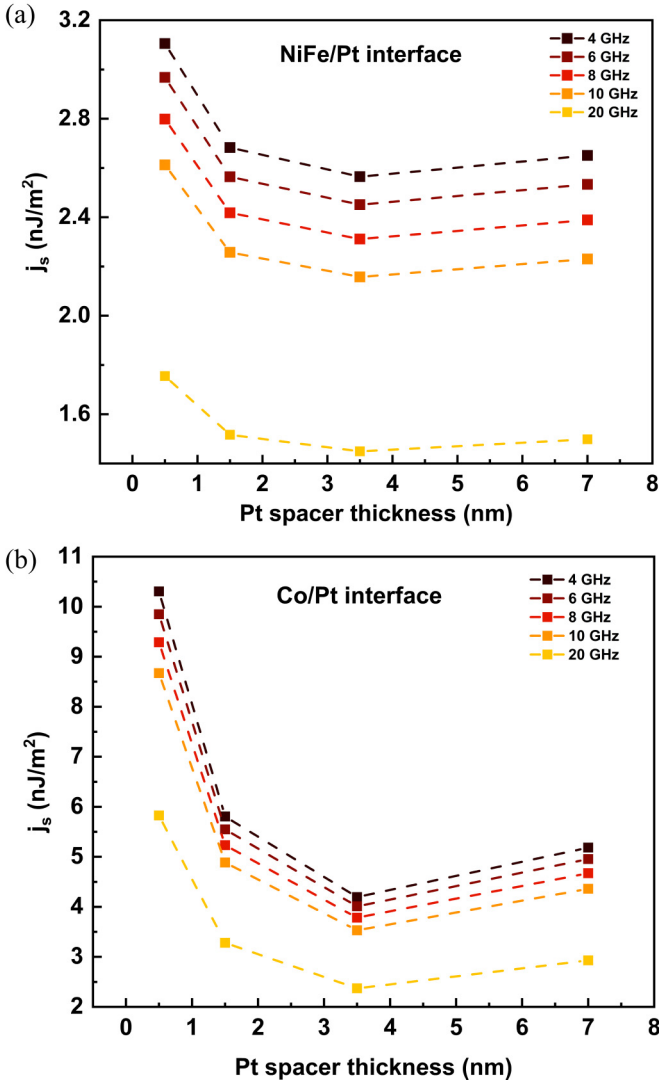

FIG. 5. Spin current density at (a) $Ni_{80}Fe_{20}$/Pt and (b) Co/Pt interface as a function of Pt spacer thickness, for different rf excitation frequencies, calculated using (12).

Here,

$$g_{\text{eff}}^{\uparrow\downarrow}(\text{Pt}) = g_{\text{eff}}^{\uparrow\downarrow}\left(1 + \left[2\sqrt{\varepsilon/3}\tanh(t_{\text{Pt}}/\lambda_{\text{sd}})\right]^{-1}\right)^{-1}, \tag{12}$$

where $g_{\text{eff}}^{\uparrow\downarrow}$ is the effective spin-mixing conductance calculated using (5) and $\varepsilon = (Z_{\text{Pt}}e^2/\hbar c)^4 = 0.1$. Note that $g_{\text{eff}}^{\uparrow\downarrow}$ does not account for the material properties of NM, in contrast to the $g_{\text{eff}}^{\uparrow\downarrow}(\text{Pt})$, calculated using Eq. (12). The estimated $j_s^{\text{FM/Pt}}$ at the Co/Pt and $Ni_{80}Fe_{20}$/Pt interfaces is shown in Fig. 5.

We see that the spin current density $j_s^{\text{FM/Pt}}$ increases with decreasing Pt thickness for both the interfaces, following the inverse dependence on α_{eff}. This trend is indicative of the enhanced backflow of spins that occurs when the $Ni_{80}Fe_{20}$ and Co layers are strongly coupled. These results can be related to the spin-pumping model discussed earlier, in that the backflow of spins is enhanced at the FM/NM interface because of the spin current pumped out of the opposing FM layer. This explains the observed increase in spin current density at the FM/Pt interface with decreasing Pt thickness. Further, the higher value of spin current density at the Co/Pt interface can be attributed to its greater interfacial spin transparency of ∼62% as compared to that of ∼25% for $Ni_{80}Fe_{20}$/Pt interface, estimated earlier. The ability to modulate the spin current density by adjusting spacer thickness and material properties thus offers a dynamic control mechanism for spin interactions for an asymmetrical trilayer system.

We observe a consistently weaker response of NiFe/Pt interface as compared to the Co/Pt interface that can be explained by considering the spin memory loss (SML) at the interface. Magnetoresistance experiments in metallic multilayers have established that spin current transfer across 3d FM/Pt interface is not 100% efficient and is subjected to SML that causes the spin current to dissipate [58,59]. The higher SML at NiFe/Pt interface can be attributed to several material and interfacial factors such as the disorder at NiFe/Pt interface because of lattice mismatch and alloying effects that enhance spin scattering [60–62], the bulk spin-orbit coupling of Pt that enhances SML even when the interfacial spin-orbit coupling is weak such as at NiFe/Pt interface [63]. Thus, the higher spin-flip scattering degrades the interfaces ability to preserve the spin-polarization of the spin current passing through it lowering the interfaces ability to transmit spin current resulting in the observed lower spin-pumping induced damping of NiFe/Pt in Fig. 4(a), in the decoupled FMs regime.

In addition to SML, spin-backflow (SBF) also governs the transfer of spin current across the interface and its contribution to spin transfer efficiency is dictated by the spin-mixing conductance of the interface [64,65].

The higher SML and lower SBF at the NiFe/Pt interface thus contributes towards lowering the interfaces spin transfer efficiency compared to Co/Pt interface which explains the consistently weaker response in the spin-pumping induced damping, interfacial spin transparency and consequently the spin current density.

VI. PHASE OF PRECESSING MAGNETIZATIONS

We further elucidate our understanding of the spin-pumping mechanism in the trilayer by analyzing it as a composite of coupled FM layers that interact through both dynamic coupling via spin pumping and static coupling via Pt-mediated exchange interactions.

To facilitate this analysis, we compute the average spin pumping induced damping ($\tilde{\alpha}_{\text{sp}}$) within the trilayer system, using the experimentally obtained saturation magnetizations (M_s) and the previously derived effective interfacial spin-mixing conductance of the two FM layers as the weighting factors, as considered in Eq. (13) below,

$$\tilde{\alpha}_{\text{sp}} = \frac{\alpha_{\text{Co}} \times M_{s,\text{Co}} \times g_{\text{eff, Co/Pt}}^{\uparrow\downarrow} + \alpha_{\text{NiFe}} \times M_{s,\text{NiFe}} \times g_{\text{eff, NiFe/Pt}}^{\uparrow\downarrow}}{M_{s,\text{Co}} \times g_{\text{eff, Co/Pt}}^{\uparrow\downarrow} + M_{s,\text{NiFe}} \times g_{\text{eff, NiFe/Pt}}^{\uparrow\downarrow}}, \tag{13}$$

with $M_{s,\text{Co}} = 1459\,\text{emu/cm}^3$ and $M_{s,\text{NiFe}} = 825\,\text{emu/cm}^3$, alongside the experimentally determined Gilbert damping parameters, α_{Co} and α_{NiFe}. The variation of the computed $\tilde{\alpha}_{\text{sp}}$ as a function of t_{Pt} is shown in Fig. 6.

The data are found to fit reasonably well to the following equation for spin pumping induced damping of the acoustic

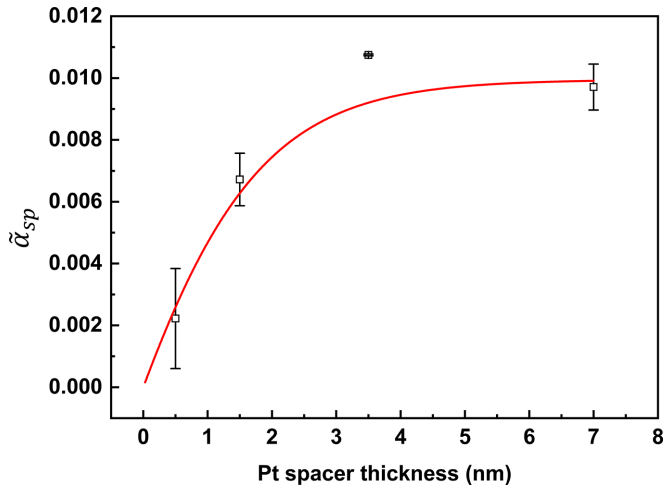

FIG. 6. Average spin pumping induced damping of the acoustic mode as a function of Pt spacer thickness. Solid red line represents fit to the data using Eq. (14).

mode [11]:

$$\tilde{\alpha}_{\rm sp} = \frac{g\mu_B}{4\pi M_s}\frac{\tilde{g}_{\uparrow\downarrow}}{t_{\rm FM}}\left[1+\frac{\tilde{g}_{\uparrow\downarrow}\mathcal{R}}{\tanh\left(\frac{t_{\rm Pt}}{2\lambda_{\rm sd}}\right)}\right]^{-1}, \qquad (14)$$

where $\mathcal{R} = \frac{\rho_\uparrow e^2}{2\pi\hbar}\lambda_{\rm sd}$, $\rho_\uparrow (= 34 \pm 1\ \mu\Omega\,{\rm cm})$ [11] is the single spin channel resistivity, $t_{\rm FM}$ is the thickness of the FM, and $g = \frac{M_{s,Co}\times g_{\rm Co}+M_{s,\rm NiFe}\times g_{\rm NiFe}}{M_{s,\rm Co}+M_{s,\rm NiFe}} = 2.15$, where $g_{\rm Co}$ and $g_{\rm NiFe}$ represent the g factors of Co and $Ni_{80}Fe_{20}$, respectively. One may note the use of the weighted average of the g factor which is necessitated by the asymmetric nature of the trilayer and the different magnetic properties of Co and NiFe. The weighted average allows us to incorporate the proportional contributions of each layer's magnetic saturation and intrinsic g factor. Consistency with the Kittel equation derived g factors for the trilayer samples, which range from 2.15 to 2.19, supports the validity of our weighted average calculation. The "'composite" spin-mixing conductance and spin-diffusion length given by $\tilde{g}_{\uparrow\downarrow}$ and λ_{sd}, respectively, are the fitting parameters. The data show a good fit to the model, suggesting that the coupled FM layers undergo in-phase acoustic mode precession. Unlike similar analyses for symmetric NiFe/Pt/NiFe trilayers [11], our asymmetric interfaces exhibit distinct behavior with a composite spin-mixing conductance, $\tilde{g}_{\uparrow\downarrow} = 1.00\times10^{20} \pm 2.9\times10^{19}{\rm m}^{-2}$ and spin -diffusion length, $\tilde{\lambda}_{\rm sd} = 2.35\times10^{-9} \pm 1.3\times10^{-10}$ m, indicating the complex magnetization dynamics at play in an asymmetrical trilayer system.

As outlined in the Introduction, magnetization precession in the coupled FM layers emits spin current out of the FM layers with parallel or opposite spin polarization, contingent upon the phase of the precessing magnetization. For NM spacer thicknesses below $\lambda_{\rm sd}$, the emitted spin current traverses the conducting Pt spacer layer via ballistic transport and is absorbed by the other FM layer [10]. Notably, for in-phase precession and $t_{\rm Pt} < \lambda_{\rm sd}$, the loss of angular momentum is mitigated by the absorption of incoming spin angular momentum, resulting in reduced spin pumping induced damping as the spacer thickness diminishes [11]. This mechanism facilitates spin pumping induced dynamic coupling between the two layers, alongside the Pt-mediated static exchange coupling. The combination of dynamic and static coupling between the FMs contributes to the observed enhancement in linewidth and shifts in the resonance field of the coupled FM layers as a function of Pt spacer thickness.

Furthermore it is important to note that, for all thicknesses of the NM layer, there is some spin backflow into the source FM that results in partial spin current scattering back into the first FM layer [66]. At the low thicknesses of the Pt spacer, when the FM layers are coupled, the loss of angular momentum is only partially mitigated, as depending on the damping and transit characteristics of all layers and interfaces in the system some losses can occur due to spin-scattering events.

VII. CONCLUSION

In summary, our systematic study of THE $Ni_{80}Fe_{20}$/Pt(t)/Co trilayer system demonstrates that variation in the Pt NM spacer thickness significantly influences the coupling of FM layers, as analyzed through VSM and macrospin simulations. An exponential decrease in the coupling strength with increasing Pt thickness is observed. Subsequently, the trilayer system with strongly coupled FM layers, with a 0.5 and 1.5 nm Pt spacer layer, exhibits a single resonance peak whereas in the systems with decoupled FM layers, for a thicker Pt spacer layer (3 and 7 nm), two well separated resonance peaks emerge, corresponding to decoupled resonances in $Ni_{80}Fe_{20}$ and Co, respectively. Spin pumping in $Ni_{80}Fe_{20}$/Pt(t)/Co studied by FMR reveals a nuanced dependency of spin pumping induced damping ($\alpha_{\rm sp}$) on the Pt spacer thickness, highlighting distinctive nonreciprocal behaviors at the $Ni_{80}Fe_{20}$/Pt and Co/Pt interfaces. The observed variation in the saturation levels of $\alpha_{\rm sp}$ for $Ni_{80}Fe_{20}$ and Co is indicative of the differential spin transport characteristics inherent to each FM/Pt interface. The effective $\alpha_{\rm sp}$ is found to decrease with decreasing Pt thickness, indicating a dynamic compensation of the spin current achieved through the in-phase precession of magnetizations in $Ni_{80}Fe_{20}$ and Co, because of the in-phase spin current pumped by the other FM layer across the thin NM spacer layer. This observation, coupled with the different values of spin-mixing conductances at the two interfaces, underscores the substantial difference in the spin current density present at two interfaces in the asymmetric trilayer system. The derived interfacial spin transparency, ∼62% for Co/Pt and ∼25% for $Ni_{80}Fe_{20}$/Pt interfaces, alongside the measured spin current densities of 10.5 nJ/m^{-2} and 3.2 nJ/m^{-2}, respectively, points out the differential spin transport efficacy across these interfaces.

This investigation establishes the foundation for addressing the theoretical integration of coupling strength and dynamic spin pumping between the FM layers for the analysis of $\alpha_{\rm sp}$ in an asymmetric trilayer system. By developing a fundamental understanding of spin pumping in an asymmetric trilayer and elucidating the function of Pt in regulating the spin transfer

dynamics this study provides a framework for future research into the mechanism of spin transport and targeted advancements in spintronic device design to improve the efficiency and performance of future applications.

ACKNOWLEDGMENTS

S.S. is thankful to Dr. Durgesh Kumar for discussion related to VSM experimental results. S.S. acknowledges receiving a Ph.D. Scholarship through Grant No. NRF-CRP21-2018-0003 from the National Research Foundation (NRF), Singapore. R.S.R. acknowledges the support from NRF, Singapore, through Grant No. NRF-CRP21-2018-0003 and the Ministry of Education, Singapore, through its Academic Research Tier 1 Grant No. RG76/22 and Tier 2 Grant No. MOE-T2EP50122-0023. Any opinions, findings, and conclusions or recommendations expressed in this material are those of the author(s) and do not reflect the views of the Ministry of Education, Singapore. Y.R. and Y.Y. are supported by the National Natural Science Foundation of China (Grant No. 62074099).

[1] S.-H. C. Baek, V. P. Amin, Y.-W. Oh, G. Go, S.-J. Lee, G.-H. Lee, K.-J. Kim, M. D. Stiles, B.-G. Park, and K.-J. Lee, Spin currents and spin-orbit torques in ferromagnetic trilayers, Nat. Mater. **17**, 509 (2018).

[2] S. I. Kiselev, J. Sankey, I. Krivorotov, N. Emley, R. Schoelkopf, R. Buhrman, and D. Ralph, Microwave oscillations of a nanomagnet driven by a spin-polarized current, Nature (London) **425**, 380 (2003).

[3] V. E. Demidov, S. Urazhdin, and S. O. Demokritov, Direct observation and mapping of spin waves emitted by spin-torque nano-oscillators, Nat. Mater. **9**, 984 (2010).

[4] A. Tulapurkar, Y. Suzuki, A. Fukushima, H. Kubota, H. Maehara, K. Tsunekawa, D. Djayaprawira, N. Watanabe, and S. Yuasa, Spin-torque diode effect in magnetic tunnel junctions, Nature (London) **438**, 339 (2005).

[5] R. Duine, K.-J. Lee, S. S. Parkin, and M. D. Stiles, Synthetic antiferromagnetic spintronics, Nat. Phys. **14**, 217 (2018).

[6] W. Legrand, D. Maccariello, F. Ajejas, S. Collin, A. Vecchiola, K. Bouzehouane, N. Reyren, V. Cros, and A. Fert, Room-temperature stabilization of antiferromagnetic skyrmions in synthetic antiferromagnets, Nat. Mater. **19**, 34 (2020).

[7] S. Wolf, D. Awschalom, R. Buhrman, J. Daughton, S. von Molnár, M. Roukes, A. Y. Chtchelkanova, and D. Treger, Spintronics: A spin-based electronics vision for the future, Science **294**, 1488 (2001).

[8] I. Žutić, J. Fabian, and S. D. Sarma, Spintronics: Fundamentals and applications, Rev. Mod. Phys. **76**, 323 (2004).

[9] Y. Tserkovnyak, Spin and charge transfer in selected nanostructures, Ph.D. thesis, Harvard University, 2003.

[10] B. Kardasz and B. Heinrich, Ferromagnetic resonance studies of accumulation and diffusion of spin momentum density in Fe/Ag/Fe/GaAs (001) and Ag/Fe/GaAs (001) structures, Phys. Rev. B **81**, 094409 (2010).

[11] P. Omelchenko, E. Girt, and B. Heinrich, Test of spin pumping into proximity-polarized Pt by in-phase and out-of-phase pumping in Py/Pt/Py, Phys. Rev. B **100**, 144418 (2019).

[12] S. O. Valenzuela and M. Tinkham, Direct electronic measurement of the spin Hall effect, Nature (London) **442**, 176 (2006).

[13] E. Saitoh, M. Ueda, H. Miyajima, and G. Tatara, Conversion of spin current into charge current at room temperature: Inverse spin-Hall effect, Appl. Phys. Lett. **88**, 182509 (2006).

[14] L. Liu, T. Moriyama, D. C. Ralph, and R. A. Buhrman, Spin-torque ferromagnetic resonance induced by the spin Hall effect, Phys. Rev. Lett. **106**, 036601 (2011).

[15] Y. Pogoryelov, M. Pereiro, S. Jana, A. Kumar, S. Akansel, M. Ranjbar, D. Thonig, D. Primetzhofer, P. Svedlindh, J. Åkerman, O. Eriksson, O. Karis, and D. A. Arena, Nonreciprocal spin pumping damping in asymmetric magnetic trilayers, Phys. Rev. B **101**, 054401 (2020).

[16] D. Huang, D. Zhang, Y. Kim, J.-P. Wang, and X. Wang, Magnetization dynamics in synthetic antiferromagnets with perpendicular magnetic anisotropy, Phys. Rev. B **107**, 214438 (2023).

[17] T. S. Parvini, E. Paz, T. Böhnert, A. Schulman, L. Benetti, F. Oberbauer, J. Walowski, F. Moradi, R. Ferreira, and M. Münzenberg, Enhancing spin-transfer torque in magnetic tunnel junction devices: Exploring the influence of capping layer materials and thickness on device characteristics, J. Appl. Phys. **133**, 24 (2023).

[18] Z. Wei, D. Navas, S. A. Bunyaev, M. Abellan, C. Garcia, G. N. Kakazei, and M. Vazquez, Static and dynamical behaviour of magnetically coupled Co/Cu/CoFeB trilayers, J. Magn. Magn. Mater. **589**, 171584 (2024).

[19] A. A. Baker, A. I. Figueroa, C. J. Love, S. A. Cavill, T. Hesjedal, and G. van der Laan, Anisotropic absorption of pure spin currents, Phys. Rev. Lett. **116**, 047201 (2016).

[20] A. Baker, A. Figueroa, L. Collins-McIntyre, G. van der Laan, and T. Hesjedal, Spin pumping in ferromagnet-topological insulator-ferromagnet heterostructures, Sci. Rep. **5**, 7907 (2015).

[21] F. Wilhelm, P. Poulopoulos, G. Ceballos, H. Wende, K. Baberschke, P. Srivastava, D. Benea, H. Ebert, M. Angelakeris, N. K. Flevaris *et al.*, Layer-resolved magnetic moments in Ni/Pt multilayers, Phys. Rev. Lett. **85**, 413 (2000).

[22] P. Omelchenko, B. Heinrich, and E. Girt, Measurements of interlayer exchange coupling of Pt in Py|Pt|Py system, Appl. Phys. Lett. **113**, 142401 (2018).

[23] C. Berk, F. Ganss, M. Jaris, M. Albrecht, and H. Schmidt, All-optical measurement of interlayer exchange coupling in Fe/Pt/FePt thin films, Appl. Phys. Lett. **112**, 052401 (2018).

[24] P. Bloemen, E. van Alphen, and W. de Jonge, Interlayer coupling in Co/Pt/Co trilayers investigated by ferromagnetic resonance, J. Magn. Magn. Mater. **104**, 1775 (1992).

[25] P. Ogrodnik, K. Grochot, Ł. Karwacki, J. Kanak, M. Prokop, J. Chęciński, W. Skowroński, S. Ziętek, and T. Stobiecki, Study of spin–orbit interactions and interlayer ferromagnetic coupling in Co/Pt/Co trilayers in a wide range of heavy-metal thickness, ACS Appl. Mater. Interfaces **13**, 47019 (2021).

[26] K. Lenz, T. Toliński, J. Lindner, E. Kosubek, and K. Baberschke, Evidence of spin-pumping effect in the ferromagnetic resonance of coupled trilayers, Phys. Rev. B **69**, 144422 (2004).
[27] S. Takahashi, Giant enhancement of spin pumping in the out-of-phase precession mode, Appl. Phys. Lett. **104**, 052407 (2014).
[28] B. Khodadadi, J. B. Mohammadi, J. M. Jones, A. Srivastava, C. Mewes, T. Mewes, and C. Kaiser, Interlayer exchange coupling in asymmetric Co−Fe/Ru/Co−Fe trilayers investigated with broadband temperature-dependent ferromagnetic resonance, Phys. Rev. Appl. **8**, 014024 (2017).
[29] A. Layadi, Effect of biquadratic coupling and in-plane anisotropy on the resonance modes of a trilayer system, Phys. Rev. B **65**, 104422 (2002).
[30] B. Heinrich, J. F. Cochran, M. Kowalewski, J. Kirschner, Z. Celinski, A. S. Arrott, and K. Myrtle, Magnetic anisotropies and exchange coupling in ultrathin fcc Co (001) structures, Phys. Rev. B **44**, 9348 (1991).
[31] B. Heinrich, Y. Tserkovnyak, G. Woltersdorf, A. Brataas, R. Urban, and G. E. W. Bauer, Dynamic exchange coupling in magnetic bilayers, Phys. Rev. Lett. **90**, 187601 (2003).
[32] B. Heinrich, G. Woltersdorf, R. Urban, and E. Simanek, Role of dynamic exchange coupling in magnetic relaxations of metallic multilayer films, J. Appl. Phys. **93**, 7545 (2003).
[33] See Supplemental Material at http://link.aps.org/supplemental/10.1103/PhysRevB.110.134440 for the x-ray characterization of the samples, the discussion of M-H hysteresis loops, details and results of the macrospin simulation, analysis of FMR spectra, the angle-dependent VSM and FMR measurements, and which includes Refs. [38,67–70].
[34] P. Bruno and C. Chappert, Oscillatory coupling between ferromagnetic layers separated by a nonmagnetic metal spacer, Phys. Rev. Lett. **67**, 1602 (1991).
[35] H. Kikuchi, J.-F. Bobo, and R. L. White, The effect of pinholes on the properties of Co/Cu multilayers, IEEE Trans. Magn. **33**, 3583 (1997).
[36] Y. Gui, A. Wirthmann, and C.-M. Hu, Foldover ferromagnetic resonance and damping in permalloy microstrips, Phys. Rev. B **80**, 184422 (2009).
[37] R. W. Damon and J. Eshbach, Magnetostatic modes of a ferromagnet slab, J. Phys. Chem. Solids **19**, 308 (1961).
[38] Y. Wei, S. Akansel, T. Thersleff, I. Harward, R. Brucas, M. Ranjbar, S. Jana, P. Lansaker, Y. Pogoryelov, and R. K. Dumas, Exponentially decaying magnetic coupling in sputtered thin film FeNi/Cu/FeCo trilayers, Appl. Phys. Lett. **106**, 042405 (2015).
[39] Z. Celinski, B. Heinrich, and J. Cochran, Ferromagnetic and antiferromagnetic exchange coupling in ultrathin Fe (001)/Pd (001)/Fe (001) structures, J. Appl. Phys. **70**, 5870 (1991).
[40] Y. Tserkovnyak, A. Brataas, and G. E. W. Bauer, Enhanced Gilbert damping in thin ferromagnetic films, Phys. Rev. Lett. **88**, 117601 (2002).
[41] J. M. Shaw, H. T. Nembach, and T. J. Silva, Determination of spin pumping as a source of linewidth in sputtered $Co_{90}Fe_{10}$/Pd multilayers by use of broadband ferromagnetic resonance spectroscopy, Phys. Rev. B **85**, 054412 (2012).
[42] R. D. McMichael, D. J. Twisselmann, and A. Kunz, Localized ferromagnetic resonance in inhomogeneous thin films, Phys. Rev. Lett. **90**, 227601 (2003).
[43] N. Behera, M. S. Singh, S. Chaudhary, D. K. Pandya, and P. Muduli, Effect of Ru thickness on spin pumping in Ru/Py bilayer, J. Appl. Phys. **117**, 17A714 (2015).
[44] H. Nakayama, K. Ando, K. Harii, T. Yoshino, R. Takahashi, Y. Kajiwara, K. Uchida, Y. Fujikawa, and E. Saitoh, Geometry dependence on inverse spin Hall effect induced by spin pumping in $Ni_{81}Fe_{19}$/Pt films, Phys. Rev. B **85**, 144408 (2012).
[45] S. Panda, S. Mondal, J. Sinha, S. Choudhury, and A. Barman, All-optical detection of interfacial spin transparency from spin pumping in β-Ta/CoFeB thin films, Sci. Adv. **5**, eaav7200 (2019).
[46] A. Brataas, Y. V. Nazarov, and G. E. W. Bauer, Finite-element theory of transport in ferromagnet–normal metal systems, Phys. Rev. Lett. **84**, 2481 (2000).
[47] A. Brataas, Y. Tserkovnyak, G. E. W. Bauer, and B. I. Halperin, Spin battery operated by ferromagnetic resonance, Phys. Rev. B **66**, 060404(R) (2002).
[48] M. Caminale, A. Ghosh, S. Auffret, U. Ebels, K. Ollefs, F. Wilhelm, A. Rogalev, and W. E. Bailey, Spin pumping damping and magnetic proximity effect in Pd and Pt spin-sink layers, Phys. Rev. B **94**, 014414 (2016).
[49] Y. You, H. Sakimura, T. Harumoto, Y. Nakamura, J. Shi, C. Song, F. Pan, and K. Ando, Study of spin mixing conductance of single oriented Pt in Pt/$Ni_{81}Fe_{19}$ heterostructure by spin pumping, AIP Adv. **11**, 035211 (2021).
[50] W. Zhang, W. Han, X. Jiang, S.-H. Yang, and S. S. P. Parkin, Role of transparency of platinum–ferromagnet interfaces in determining the intrinsic magnitude of the spin Hall effect, Nat. Phys. **11**, 496 (2015).
[51] L. Zhu, D. C. Ralph, and R. A. Buhrman, Effective spin-mixing conductance of heavy-metal–ferromagnet interfaces, Phys. Rev. Lett. **123**, 057203 (2019).
[52] M. Obstbaum, M. Härtinger, H. G. Bauer, T. Meier, F. Swientek, C. H. Back, and G. Woltersdorf, Inverse spin Hall effect in $Ni_{81}Fe_{19}$/normal-metal bilayers, Phys. Rev. B **89**, 060407(R) (2014).
[53] O. Mosendz, V. Vlaminck, J. E. Pearson, F. Y. Fradin, G. E. W. Bauer, S. D. Bader, and A. Hoffmann, Detection and quantification of inverse spin Hall effect from spin pumping in permalloy/normal metal bilayers, Phys. Rev. B **82**, 214403 (2010).
[54] H. J. Jiao and G. E. W. Bauer, Spin backflow and ac voltage generation by spin pumping and the inverse spin Hall effect, Phys. Rev. Lett. **110**, 217602 (2013).
[55] A. Azevedo, L. Vilela-Leão, R. Rodríguez-Suárez, A. L. Santos, and S. Rezende, Spin pumping and anisotropic magnetoresistance voltages in magnetic bilayers: Theory and experiment, Phys. Rev. B **83**, 144402 (2011).
[56] T. Fache, J. Rojas-Sanchez, L. Badie, S. Mangin, and S. Petit-Watelot, Determination of spin Hall angle, spin mixing conductance, and spin diffusion length in CoFeB/Ir for spin-orbitronic devices, Phys. Rev. B **102**, 064425 (2020).
[57] S. Husain, A. Kumar, V. Barwal, N. Behera, S. Akansel, P. Svedlindh, and S. Chaudhary, Spin pumping in ion-beam sputtered Co_2FeAl/Mo bilayers: Interfacial Gilbert damping, Phys. Rev. B **97**, 064420 (2018).
[58] K. Eid, D. Portner, J. A. Borchers, R. Loloee, M. A.-H. Darwish, M. Tsoi, R. D. Slater, K. V. O'Donovan, H. Kurt, W. P. Pratt, Jr., and J. Bass, Absence of mean-free-path effects in the

current-perpendicular-to-plane magnetoresistance of magnetic multilayers, Phys. Rev. B **65**, 054424 (2002).

[59] J.-C. Rojas-Sánchez, N. Reyren, P. Laczkowski, W. Savero, J.-P. Attané, C. Deranlot, M. Jamet, J.-M. George, L. Vila, and H. Jaffrès, Spin pumping and inverse spin Hall effect in platinum: The essential role of spin-memory loss at metallic interfaces, Phys. Rev. Lett. **112**, 106602 (2014).

[60] R. Liu, K. Gupta, Z. Yuan, and P. J. Kelly, Calculating the spin memory loss at Cu|metal interfaces from first principles, Phys. Rev. B **106**, 014401 (2022).

[61] S. Azzawi, A. Ganguly, M. Tokaç, R. Rowan-Robinson, J. Sinha, A. Hindmarch, A. Barman, and D. Atkinson, Evolution of damping in ferromagnetic/nonmagnetic thin film bilayers as a function of nonmagnetic layer thickness, Phys. Rev. B **93**, 054402 (2016).

[62] C. Swindells, A. Hindmarch, A. Gallant, and D. Atkinson, Spin transport across the interface in ferromagnetic/nonmagnetic systems, Phys. Rev. B **99**, 064406 (2019).

[63] M. Lim and H.-W. Lee, Spin-memory loss induced by bulk spin–orbit coupling at ferromagnet/heavy-metal interfaces, Appl. Phys. Lett. **118**, 042408 (2021).

[64] P. M. Haney, H.-W. Lee, K.-J. Lee, A. Manchon, and M. D. Stiles, Current induced torques and interfacial spin-orbit coupling: Semiclassical modeling, Phys. Rev. B **87**, 174411 (2013).

[65] V. P. Amin and M. D. Stiles, Spin transport at interfaces with spin-orbit coupling: Phenomenology, Phys. Rev. B **94**, 104420 (2016).

[66] L. Zhu, D. C. Ralph, and R. A. Buhrman, Maximizing spin-orbit torque generated by the spin Hall effect of Pt, Appl. Phys. Rev. **8**, 031308 (2021).

[67] A. Natarajarathinam, Z. Tadisina, T. Mewes, S. Watts, E. Chen, and S. Gupta, Influence of capping layers on CoFeB anisotropy and damping, J. Appl. Phys. **112**, 5 (2012).

[68] H. Meng, W. Lum, R. Sbiaa, S. Lua, and H. Tan, Annealing effects on CoFeB-MgO magnetic tunnel junctions with perpendicular anisotropy, J. Appl. Phys. **110**, 033904 (2011).

[69] N. Nakajima, T. Koide, T. Shidara, H. Miyauchi, H. Fukutani, A. Fujimori, K. Iio, T. Katayama, M. Nývlt, and Y. Suzuki, Perpendicular magnetic anisotropy caused by interfacial hybridization via enhanced orbital moment in Co/Pt multilayers: Magnetic circular x-ray dichroism study, Phys. Rev. Lett. **81**, 5229 (1998).

[70] B. Zhang, A. Cao, J. Qiao, M. Tang, K. Cao, X. Zhao, S. Eimer, Z. Si, N. Lei, Z. Wang *et al.*, Influence of heavy metal materials on magnetic properties of Pt/Co/heavy metal tri-layered structures, Appl. Phys. Lett. **110**, 012405 (2017).